Title

Residual analysis of the water resonance signal in breast lesions imaged with high spectral and spatial resolution (HiSS) MRI: A pilot study

Journal

Medical Physics, 41(1)

ISSN

0094-2405

Authors

Weiss, William A
Medved, Milica
Karczmar, Gregory S
et al.

Publication Date

2014-01-02

DOI

10.1118/1.4851615

Peer reviewed

Residual analysis of the water resonance signal in breast lesions imaged with high spectral and spatial resolution (HiSS) MRI: A pilot study

William A. Weiss,[a] Milica Medved, Gregory S. Karczmar, and Maryellen L. Giger
Department of Radiology, The University of Chicago, 5841 South Maryland Avenue, Chicago, Illinois 60637

(Received 13 June 2013; revised 7 November 2013; accepted for publication 4 December 2013; published 2 January 2014)

Purpose: High spectral and spatial resolution magnetic resonance imaging (HiSS MRI) yields information on the local environment of suspicious lesions. Previous work has demonstrated the advantages of HiSS (complete fat-suppression, improved image contrast, no required contrast agent, etc.), leading to initial investigations of water resonance lineshape for the purpose of breast lesion classification. The purpose of this study is to investigate a quantitative imaging biomarker, which characterizes non-Lorentzian components of the water resonance in HiSS MRI datasets, for computer-aided diagnosis (CADx).
Methods: The inhomogeneous broadening and non-Lorentzian or "off-peak" components seen in the water resonance of proton spectra of breast HiSS images are analyzed by subtracting a Lorentzian fit from the water peak spectra and evaluating the difference spectrum or "residual." The maxima of these residuals (referred to hereafter as "off-peak components") tend to be larger in magnitude in malignant lesions, indicating increased broadening in malignant lesions. The authors considered only those voxels with the highest magnitude off-peak components in each lesion, with the number of selected voxels dependent on lesion size. Our voxel-based method compared the magnitudes and frequencies of off-peak components of all voxels from all lesions in a database that included 15 malignant and 8 benign lesions (yielding ~3900 voxels) based on the lesions' biopsy-confirmed diagnosis. Lesion classification was accomplished by comparing the average off-peak component magnitudes and frequencies in malignant and benign lesions. The area under the ROC curve (AUC) was used as a figure of merit for both the voxel-based and lesion-based methods.
Results: In the voxel-based task of distinguishing voxels from malignant and benign lesions, off-peak magnitude yielded an AUC of 0.88 (95% confidence interval [0.84, 0.91]). In the lesion-based task of distinguishing malignant and benign lesions, average off-peak magnitude yielded an AUC 0.83 (95% confidence interval [0.61, 0.98]).
Conclusions: These promising AUC values suggest that analysis of the water-resonance in each HiSS image voxel using "residual analysis" could have high diagnostic utility and could be used to enhance current CADx methods and allow detection of breast cancer without the need to inject contrast agents.
 [http://dx.doi.org/10.1118/1.4851615]

Key words: echo planar spectroscopic imaging (EPSI), breast computer-aided diagnosis, lesion classification, water resonance lineshape, spectroscopic imaging

1. INTRODUCTION

It is estimated that 232 340 women will have been diagnosed with and 39 620 women will die of breast cancer in 2013;[1] thus there is a need for early and accurate detection of breast cancer. Magnetic resonance imaging (MRI) is increasingly being investigated as a screening tool, especially for those women at greater lifetime risk.[2]

Dynamic contrast enhanced MRI (DCEMRI) using a gadolinium-based contrast agent is often employed to enhance sensitivity to breast lesions.[2,3] Contrast enhancement curves provide local physiological and microvasculature information which can increase the specificity of the scan. Characteristic uptake and washout patterns may be utilized by the radiologist in computer-aided diagnosis (CADx) of breast lesions.[4] The administration of contrast agent, however, introduces undesirable risks. The injection itself is invasive, presenting potential complications such as infection, bruising, and bleeding. A doctor or nurse must be present to deal with potential allergic reactions to the agent, and for those patients with compromised renal function, the toxicity of Gadolinium can lead to nephrogenic systemic fibrosis (NSF).[5] As MRI is being more frequently used for screening, intravenous contrast injection becomes impractical and carries too high a risk for screening large numbers of women. Therefore, a contrast-free MRI method is desirable.

High spectral and spatial resolution (HiSS) MRI can be implemented as a noncontrast enhanced, echo planar spectroscopic imaging [EPSI (Refs. 6 and 7)] technique which uses a rapidly alternating readout gradient that allows both spatial and temporal data to be recorded simultaneously. A series of gradient echo images are acquired with a temporal resolution on the order of milliseconds, rapid enough to capture the full bandwidth of the free-induction decay (FID) in each voxel of the image. The FID in each image voxel can be processed to produce a proton resonance spectrum. Magnetic

resonance spectroscopic imaging (MRSI) had been applied to breast cancer imaging, where images of low concentrations of metabolites are produced with large (~1 cc) voxels.[8] By contrast, HiSS produces images of specific components of the water or fat resonance, in small voxels, at the spatial resolution typical of conventional imaging methods. Signals from metabolites that are present at the millimolar level are generally not resolvable with the high spatial resolution of HiSS. However, the detailed structure of the water resonances detectable in HiSS data are an important source of information about local physiology.[9–11]

Images can be created from HiSS data in which the value of each voxel is proportional to the amplitude of an individual spectral component. Using spectral postprocessing, HiSS water-peak-height images produce fat suppression that is superior relative to conventional fat suppression techniques, without the disadvantages associated with fat suppression pulses.[12–14] Construction of an image from a single component of the water resonance reduces blurring due to chemical shift effects and results in higher quality images.[15] In preliminary studies, 2D HiSS water-peak-height images yielded performance similar to that of 2D and 3D dynamic contrast-enhanced (DCE) MRI in separating benign from malignant lesions.[16,17] Other work has explored variations in image contrast in images produced from different spectral components of the water resonance (obtained from HiSS data) and their relevance to the diagnosis of lesions, with promising results.[12,18,19]

Non-Lorentzian inhomogeneous broadening is often observed in the water resonance in small voxels.[9–11,14,18–20] This indicates subvoxelar environmental effects that cannot be resolved with conventional MRI, in which all spectral components of the water resonance combine in the time domain to produce a single complex value associated with each image voxel. Non-Lorentzian, or "off-peak," components are often a product of local magnetic susceptibility differences likely due to inhomogeneous blood deoxyhemoglobin levels as well as other sources of magnetic susceptibility gradients (e.g., microcalcifications). Non-Lorentzian features can also be due to differences in the exchange rate of various Fourier components of the water resonance with bound pools of water.

The magnitude and/or spectral location of these off-peak components correlate with malignancy of breast lesions.[18–20] Malignant lesions tend to contain increased levels of deoxygenated blood,[21] motivating the hypothesis that malignant lesions may display larger, asymmetric broadening of the water resonance. A previous study identified off-peak components by finding the maximum of a residual spectrum after subtracting a Lorentzian fit[19] from spectra from voxels with water-peak height above a noise threshold. It was found that malignant lesions tend to contain off-peak components at larger positive frequency offsets, though no significant correlation was found between off-peak component magnitude and malignancy.

The previous analysis, however, included many off-peak components with amplitudes close to the noise level. These components contribute little to the classification of breast lesions, as both malignant and benign lesions may contain low-magnitude off-peak components. We modified this approach by further processing the data to include in each lesion only the largest magnitude off-peak components having positive frequency offsets. Our approach seeks to eliminate off-peak components whose magnitudes are near the noise level, thus increasing the signal-to-noise ratio (SNR) of the off-peak components used in the classification of breast lesions.

2. MATERIALS AND METHODS

Figure 1 illustrates our overall analysis method of obtaining a quantitative imaging biomarker, which characterizes non-Lorentzian components of the water resonance in HiSS MRI datasets, for computer-aided diagnosis (CADx).

2.A. Data acquisition and database

In the acquisition of HiSS data, an alternating readout gradient was used to encode time-domain data using echo-planar spectroscopic imaging (EPSI). To reconstruct HiSS images, the k-space data were Fourier transformed to produce images with two spatial dimensions and one spectral dimension. In-house software was developed to automatically identify the water peak in each spectrum. Images were then created in which the value of each voxel corresponds to the peak value of the water resonance [water-peak height images, Fig. 1(b)].

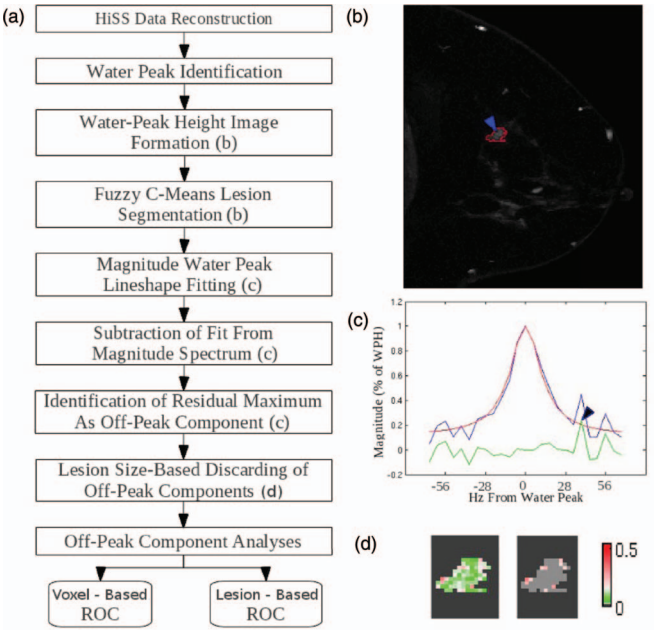

FIG. 1. (a) Flowchart outlining the off-peak component analysis. The letters in parentheses refer to parts (b), (c), and (d) of this figure, which contain representative images of the given step (see text for details of each step). (b) Water-peak height image of a breast containing an IDC grade II tumor. The fuzzy c-means segmented lesion is shown in red. (c) Water resonance originating from the voxel highlighted by the blue arrow in (b). The blue spectrum is the original resonance normalized to the water-peak height and the red spectrum is its least-squares Lorentzian fit. The residual spectrum (original resonance-Lorentzian fit) is shown in green. The black arrow points to the maximum of the residual (labeled as the "off-peak component"). (d) Map of the off-peak component magnitudes for all voxels in the lesion (left) and the corresponding map after removing voxels with low magnitude offpeak components (right).

All data were acquired on a 1.5 T Philips Achieva MR scanner (Philips Healthcare, Andover, MA). Single-slice sagittal acquisitions were performed with in-plane resolution of 1 mm in a 512 × 256 mm^2 field-of-view, 2 mm slice thickness, TR = 500 ms, effective TE = 90 ms, flip angle = 90°, echo train length = 128, spectral resolution/bandwidth = 5.6 Hz/716.8 Hz, and automatic shimming.

The 2D HiSS image data were collected retrospectively and included 23 lesions from 23 patients with biopsy-proven diagnoses. These lesions included: 15 malignant lesions (eight IDC's with associated DCIS, five IDC, one invasive mucinous cancer, one adenoid cystic carcinoma), and eight benign lesions (seven fibroadenomas and one fat necrosis). Data for this project had been acquired with informed consent from each patient, under an institutional review board-approved protocol and in compliance with the Health Insurance Portability and Accountability Act.

2.B. Lesion segmentation

Lesion segmentation was performed using an automatic 2-class (lesion and nonlesion) fuzzy c-means (FCM) (Refs. 17 and 22) algorithm on a manually drawn, rectangular region of the water-peak height image containing the lesion [Fig. 1(b)]. The water resonance peak intensity from each voxel of the ROI serves as input to the FCM algorithm. Class-membership weighting is initially assigned to each voxel as "lesion" or "nonlesion" (summing to 1). The membership weightings are then iteratively updated until the interclass variation is maximized and the intraclass variation is minimized. The class with the largest water resonance is then labeled as the "lesion" class, and voxels with a membership weight above 0.4 in that class are considered to be within the lesion.

2.C. Off-peak component analysis

After normalizing to the water-peak height, off-peak component analysis was conducted on the magnitude spectrum in each voxel within the lesion following the procedure outlined in Fig. 1. Since normalizing spectra to the water-peak height amplifies noise, we only included voxels with water-peak heights at least four times the noise level of the spectrum. The noise level was determined by finding the root-mean-squared value of a 56 Hz (10 spectral bins) area of the spectrum between the water and fat resonances; a spectral frequency region assumed to contain only noise.

We define an off-peak component as the largest non-Lorentzian feature of a spectrum; therefore, a magnitude-Lorentzian line shape was fit to and subtracted from the normalized spectrum. The nonlinear least squares fit was performed over a frequency range of 134.4 Hz, centered on the water peak, in order to capture the water resonance while excluding areas of the spectrum that were primarily baseline noise. The remaining residual spectrum then contains the non-Lorentzian components of the normalized water resonance [Fig. 1(c)]. Because earlier work revealed that off-peak components tended to be positively shifted in malignant lesions,[19] our analysis focused solely on non-Lorentzian spectral features with positive frequency shifts relative to the peak of the water resonance—specifically, only residual maxima in the range [22.4 Hz, 67.2 Hz] from the water peak were considered. This range of frequencies was chosen because below an offset of 22.4 Hz, the off-peak components are not well-resolved from the main peak.

Off-peak components are often inhomogeneous in magnitude within a lesion, probably due to the spatial inhomogeneity of, for example, tissue oxygenation and angiogenesis. In fact, both benign and malignant lesions tend to contain many (and often mostly) voxels with low off-peak component magnitudes. This may at first suggest that off-peak component magnitudes are inadequate as a lesion classifier; however, we observed that malignant lesions tended to contain greater numbers of relatively large magnitude off-peak components than did benign lesions. Thus, in this work, we applied a "voxel elimination" step, based on the relative intensity of the off-peak components. We retained for analysis the voxels with the largest 10% off-peak components in a lesion, but not less than 10 and no more than 50 voxels [Fig. 1(d)]. The 10% cutoff was selected as a trade-off between increased algorithm performance and preserving enough relevant voxels for meaningful statistical analysis. Classifier analysis was conducted on the voxels that remained after the off-peak components with lower magnitudes were eliminated.

2.D. Evaluation and statistical analysis

Data processing was performed using MatLab (The MathWorks, Inc., Natick, MA) and ROC-Kit (University of Chicago, http://metz-roc.uchicago.edu/). Area under the ROC curve (AUC) was used as the metric for assessing the performance of the four classification tasks: *voxel*-based classification using the off-peak magnitude of voxels within the lesions before and after voxel elimination, *voxel-based* classification using the off-peak frequency shift (i.e., the frequency difference between the main water peak and the off-peak component) after voxel elimination, and *lesion-based* classification using average off-peak magnitude and average off-peak frequency shift after voxel elimination. To investigate whether off-peak magnitude voxel classification performance varied across frequency offsets, AUC values were also generated postvoxel elimination considering voxels with off-peak component at each frequency shift.

3. RESULTS

3.A. Voxel-based performance

Figure 2 compares the off-peak components from all lesions (~8500 voxels) with those remaining after the low-off-peak-magnitude voxel elimination process (~550 voxels), using box plots of the off-peak magnitude versus frequency offset. After low signal-to-noise ratio voxel elimination, the substantial upward shift of the off-peak component magnitudes from malignant lesions, with the much less pronounced shift of those from benign lesions, corresponds to the increase in voxel-based AUC on off-peak magnitude from 0.65 to 0.88 (95% confidence interval [0.84, 0.91]), for all spectral

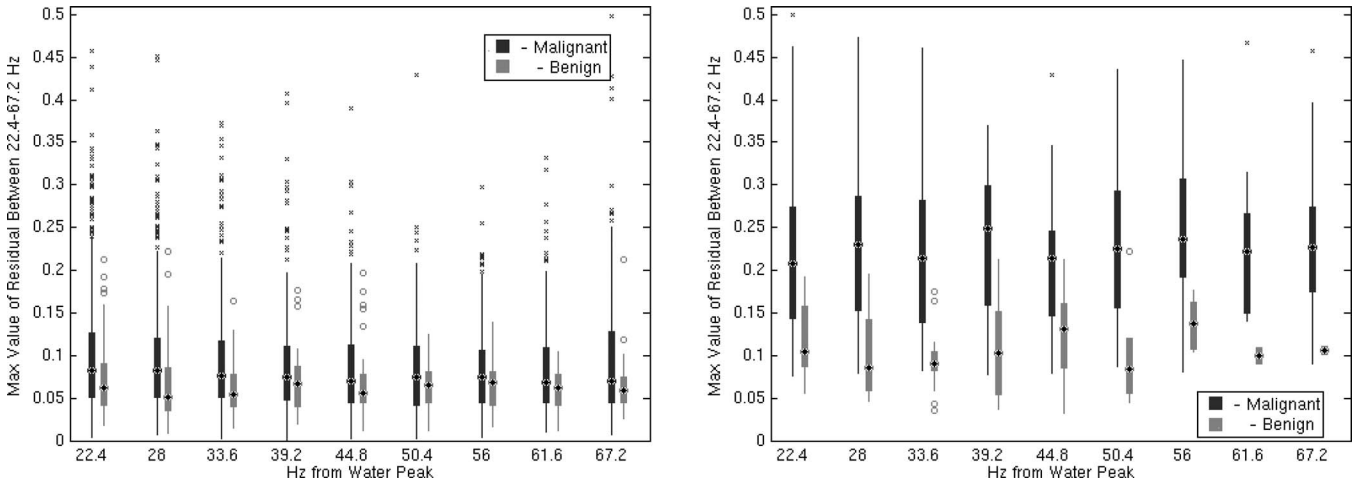

FIG. 2. Box-and-whisker plots of off-peak component magnitude vs frequency offset considering all voxels in all lesions (left) and only those voxels retained after discarding low magnitude off-peak components from each lesion (right). The median of the distribution of malignant off-peak magnitudes at each frequency offset shifts upwards considerably after voxel elimination, indicating improvement in distinguishing off-peak components from malignant and benign lesions. The distributions across frequency offset do not change appreciably. A slight offset along the x-axis is used in the plot to clearly distinguish voxels from benign and malignant lesions.

frequency bins combined. To examine whether a specific frequency offset (or range of offsets) performed better than the aggregate, ROC analysis was also performed on the off-peak magnitudes at each offset. The results are presented in Table I, where the 95% confidence intervals for individual frequency offsets are shown to overlap with the aggregate CI for most offsets. The high AUCs at larger offsets are likely due to the small number of samples input to ROC analysis and are most likely artificial.

Voxel-based ROC analysis of off-peak component frequency offsets yields an AUC of 0.51 (95% C.I. [0.43, 0.55]); therefore, this pilot study showed no relationship between malignancy and off-peak frequency. The ROC curves generated for the task of classifying voxels from malignant from benign lesions based on off-peak magnitude and off-peak frequency offset are presented in Fig. 4.

3.B. Lesion-based performance

Figure 3 shows the distributions of average off-peak magnitude and average off-peak frequency shift for both malignant and benign lesions. The AUC generated from the magnitude distributions is 0.83 (95% C.I. [0.61, 0.98]), indicating promising performance in classifying malignant and benign lesions. Average frequency offset did not perform well, with an AUC of only 0.55 (95% C.I. [0.27, 0.83]). The ROC curves generated for the task of classifying malignant from benign lesions based on average off-peak magnitude and average off-peak frequency offset are presented in Fig. 4.

4. DISCUSSION

From Fig. 2, it is apparent that the off-peak component magnitude distributions from malignant and benign lesions have similar medians, but that they are much more homogeneous in benign than in malignant lesions. Malignant lesions tend to contain a larger minority of voxels with very large off-peak component magnitudes. These largest-magnitude voxels motivated our analysis.

A previous investigation reported that off-peak component magnitude did not adequately distinguish malignant from benign lesions,[19] but that a correlation existed between malignancy and off-peak component location. However, here we took a different approach and maximized the signal-to-noise ratio of the evaluated features by selecting only the largest off-peak non-Lorentzian components in each lesion. In addition, we evaluated only off-peak components at frequencies greater than 22.4 Hz above the water resonance. Using this limited range, we failed to show any significant correlation between off-peak frequency *offset* and malignancy. Thus, in our approach, only the *magnitude* of off-peak components enabled the classification of breast lesions.

An AUC of 0.5 corresponds to choosing a random classification, while an AUC of 1.0 indicates a perfect classifier.

TABLE I. Results of ROC analysis on the classification of voxels from malignant vs benign lesions considering off-peak component magnitudes separately at each spectral frequency location (Hz from water peak) and for all bins together.

Spectral frequency (Hz from water peak)	22.4	28	33.6	39.2	44.8	50.4	56	61.6	67.2	All
No. of voxels	127	102	71	62	59	40	40	27	31	559
AUC	0.82	0.91	0.89	0.88	0.85	0.90	0.86	1.00	0.95	0.88
95% C.I.	[0.74, 0.90]	[0.79, 1.00]	[0.81, 0.97]	[0.80, 0.96]	[0.73, 0.97]	[0.74, 1.00]	[0.74, 0.98]	[1.00, 1.00]	[0.87, 1.00]	[0.84, 0.92]

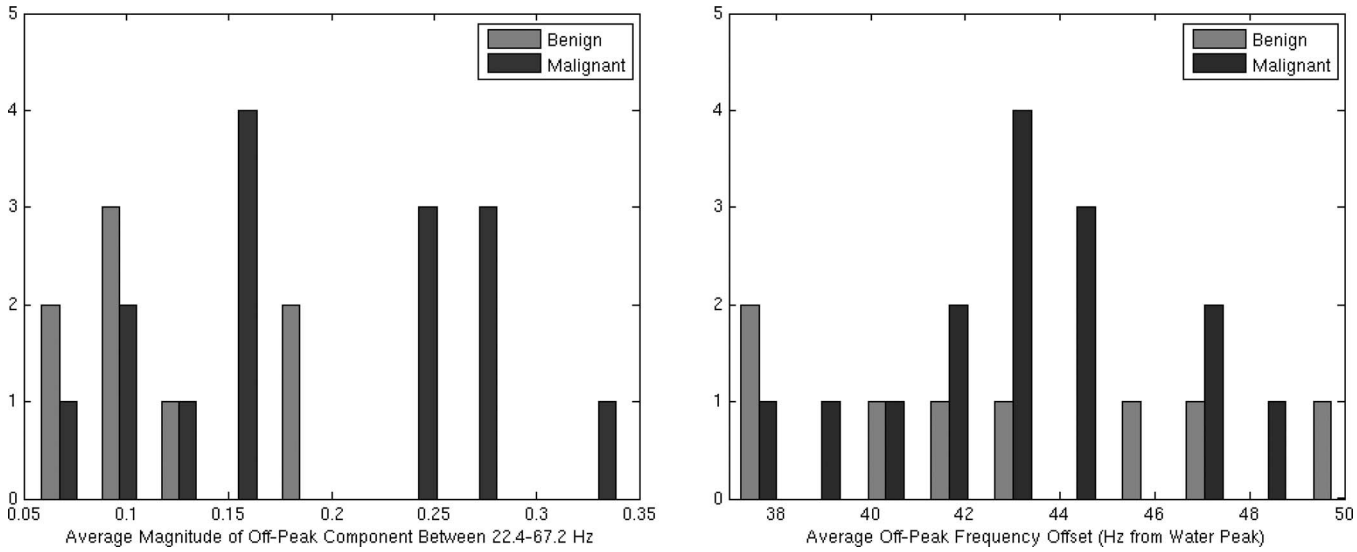

FIG. 3. Distribution of average off-peak component magnitudes (left) and of average off-peak component frequency shifts (right) across all cases included in this study.

These AUC's correspond to an ROC curve with a slope of 1 from the origin and an ROC curve with slope zero across the top of the plot, respectively. The performance of *off-peak frequency offset*, for both voxel-based and lesion-based classifiers (AUC of 0.51 and 0.55, respectively) performed similarly to randomly assigning a classification. However, the 95% confidence intervals for AUCs generated for *off-peak magnitude* for both voxel-based and lesion-based classifiers (AUC of 0.88 and 0.83, respectively) do not include 0.5, indicating that our result is statistically significant.

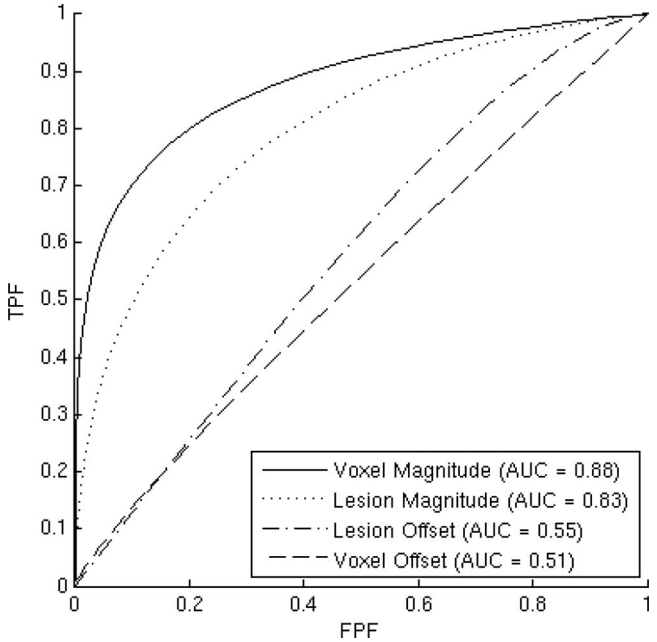

FIG. 4. ROC curves describing the performance of off-peak magnitude and frequency offset in distinguishing voxels from malignant lesions and those from benign lesions and the performance in distinguishing malignant and benign lesions based on averaged voxel values. In our study, off-peak magnitude performs well in the task of classifying both voxels and lesions, while off-peak frequency offset does not.

While the results of this pilot study are promising, there are several possible areas for improvement by future studies. Our database, while small (n = 23 lesions), was sufficient to assess the classification potential and feasibility of our analysis method, but a higher number of cases is desired. Ideally, every acquisition should image the entire 3D lesion; however, because of scan-time limitations, we were restricted to a single 2D slice. This should not be too limiting though, as a previous study[17] compared single-slice 2D HiSS data with 3D DCEMRI data of the entire lesions and found that they performed similarly in the lesion classification task. Work has been performed[23] to use sensitivity encoding (SENSE) to accelerate HiSS acquisitions, and in the future it will allow acquisition of high resolution data from multiple slices. Acquisition at 3.0T instead of 1.5T would increase the signal-to-noise ratio (SNR) of our acquired data. This could make low-magnitude off-peak components of water spectra more readily visible. Frequency shifts due to magnetic susceptibility would also be greater at higher field strength, so off-peak components may become better resolved from the main water peak.

5. CONCLUSION

In conclusion, we have shown that off-peak components of water-resonance spectra originating from voxels within malignant breast lesions often have larger magnitudes relative to their water-peak height than those within benign lesions. We have developed an automated method of identifying these largest off-peak components within HiSS-imaged breast lesions. Our method also automatically extracts the average of these largest off-peak components' magnitudes within a lesion as a means to classify lesions as malignant or benign. We have shown that features extracted from HiSS

data can be quite effective in separating malignant from benign lesions even though HiSS images are acquired without an injected contrast agent. In the future, it may be possible to combine these methods as well as other noncontrast breast MR imaging methods (e.g., DWI) to further improve accuracy of noncontrast-enhanced (e.g., screening and/or diagnostic) breast MRI exams.

ACKNOWLEDGMENTS

This work is supported in parts by NIH T32 EB002103-22, S10 RR021039, and R01 CA167785.

[a]Author to whom correspondence should be addressed. Electronic mail: willw00@uchicago.edu

[1]*SEER Cancer Statistics Review, 1975–2009 (Vintage 2009 Populations)*, edited by N. Howlader, A. M. Noone, M. Krapcho, N. Neyman, R. Aminou, S. F. Altekruse, C. L. Kosary, J. Ruhl, Z. Tatalovich, H. Cho, A. Mariotto, M. P. Eisner, D. R. Lewis, H. S. Chen, E. J. Feuer, and K. A. Cronin (National Cancer Institute, Bethesda, MD, 2012).

[2]D. Saslow, C. Boetes, W. Burke, S. Harms, M. O. Leach, C. D. Lehman, E. Morris, E. Pisano, M. Schnall, S. Sener, R. A. Smith, E. Warner, M. Yaffe, K. S. Andrews, and C. A. Russell, "American Cancer Society guidelines for breast screening with MRI as an adjunct to mammography," Ca-Cancer J. Clin. **57**(2), 75–89 (2007).

[3]M. J. Paldino and D. P. Barboriak, "Fundamentals of quantitative dynamic contrast-enhanced MR imaging," Magn. Reson. Imaging Clin. N. Am. **17**(2), 277–289 (2009).

[4]W. Chen, M. L. Giger, U. Bick, and G. M. Newstead, "Automatic identification and classification of characteristic kinetic curves of breast lesions on DCE-MRI," Med. Phys. **33**(8), 2878–2887 (2006).

[5]P. H. Kuo, E. Kanal, A. K. Abu-Alfa, and S. E. Cowper, "Gadolinium-based MR contrast agents and nephrogenic systemic fibrosis," Radiology **242**(3), 647–649 (2007).

[6]P. Mansfield, "Spatial mapping of the chemical shift in NMR," Magn. Reson. Med. **1**(3), 370–386 (1984).

[7]R. V. Mulkern and L. P. Panych, "Echo planar spectroscopic imaging," Concepts Magn. Reson. **13**(4), 213–237 (2001).

[8]M. A. Jacobs, P. B. Barker, P. A. Bottomley, Z. Bhujwalla, and D. A. Bluemke, "Proton magnetic resonance spectroscopic imaging of human breast cancer: A preliminary study," J. Magn. Reson. Imaging **19**(1), 68–75 (2004).

[9]W. Du, Y. P. Du, U. Bick, X. Fan, P. M. MacEneaney, M. A. Zamora, M. Medved, and G. S. Karczmar, "Breast MR imaging with high spectral and spatial resolutions: Preliminary experience," Radiology **224**(2), 577–585 (2002).

[10]S. Foxley, X. Fan, D. Mustafi, C. Yang, M. A. Zamora, M. Medved, and G. S. Karczmar, "Quantitative analysis of water proton spectral lineshape: A novel source of contrast in MRI," Phys. Med. Biol. **53**(17), 4509–4522 (2008).

[11]S. Foxley, X. Fan, D. Mustafi, C. Haney, M. Zamora, E. Markiewicz, M. Medved, A. M. Wood, and G. S. Karczmar, "Sensitivity to tumor microvasculature without contrast agents in high spectral and spatial resolution MR images," Magn. Reson. Med. **61**(2), 291–298 (2009).

[12]M. Medved, W. Du, M. A. Zamora, X. Fan, O. I. Olopade, P. M. MacEneaney, G. Newstead, and G. S. Karczmar, "The effect of varying spectral resolution on the quality of high spectral and spatial resolution magnetic resonance images of the breast," J. Magn. Reson. Imaging. **18**(4), 442–448 (2003).

[13]X. Fan, H. Abe, M. Medved, S. Foxley, S. Arkani, M. A. Zamora, O. I. Olopade, G. M. Newstead, and G. S. Karczmar, "Fat suppression with spectrally selective inversion vs. high spectral and spatial resolution MRI of breast lesions: Qualitative and quantitative comparisons," J. Magn. Reson. Imaging **24**(6), 1311–1315 (2006).

[14]M. Medved, G. M. Newstead, H. Abe, O. I. Olopade, A. Shimauchi, M. A. Zamora, and G. S. Karczmar, "Clinical implementation of a multislice high spectral and spatial resolution-based MRI sequence to achieve unilateral full-breast coverage," Magn. Reson. Imaging **28**(1), 16–21 (2010).

[15]M. Medved, G. M. Newstead, H. Abe, M. A. Zamora, O. I. Olopade, and G. S. Karczmar, "High spectral and spatial resolution MRI of breast lesions: Preliminary clinical experience," Am. J. Roentgenol. **186**(1), 30–37 (2006).

[16]M. Medved, X. Fan, H. Abe, G. M. Newstead, A. M. Wood, A. Shimauchi, K. Kulkarni, M. K. Ivancevic, L. L. Pesce, O. I. Olopade, and G. S. Karczmar, "Non-contrast enhanced MRI for evaluation of breast lesions: Comparison of non-contrast enhanced high spectral and spatial resolution (HiSS) images versus contrast enhanced fat-suppressed images," Acad. Radiol. **18**(12), 1467–1474 (2011).

[17]N. Bhooshan, M. Giger, M. Medved, H. Li, A. Wood, Y. Yuan, L. Lan, A. Marquez, G. Karczmar, and G. Newstead, "Potential of computer-aided diagnosis of high spectral and spatial resolution (HiSS) MRI in the classification of breast lesions: HiSS MRI CADx in breast lesion classification," J. Magn. Reson. Imaging **39**(1), 59–67 (2013).

[18]M. Medved, G. M. Newstead, X. Fan, Y. P. Du, O. I. Olopade, A. Shimauchi, M. A. Zamora, and G. S. Karczmar, "Fourier component imaging of water resonance in human breast provides markers for malignancy," Phys. Med. Biol. **54**(19), 5767–5779 (2009).

[19]A. M. Wood, M. Medved, I. D. Bacchus, H. A. Al-Hallaq, A. Shimauchi, G. M. Newstead, O. I. Olopade, S. S. Venkataraman, M. K. Ivancevic, and G. S. Karczmar, "Classification of breast lesions pre-contrast injection using water resonance lineshape analysis," NMR Biomed. **26**(5), 569–577 (2012).

[20]M. Medved, G. M. Newstead, X. Fan, W. Du, Y. P. Du, P. M. MacEneaney, R. M. Culp, F. Kelcz, O. I. Olopade, M. A. Zamora, and G. S. Karczmar, "Fourier components of inhomogeneously broadened water resonances in breast: A new source of MRI contrast," Magn. Reson. Med. **52**(1), 193–196 (2004).

[21]H. A. Al-Hallaq, X. Fan, M. Zamora, J. N. River, J. E. Moulder, and G. S. Karczmar, "Spectrally inhomogeneous BOLD contrast changes detected in rodent tumors with high spectral and spatial resolution MRI," NMR Biomed. **15**(1), 28–36 (2002).

[22]J. C. Bezdek, R. Ehrlich, and W. Full, "FCM: The fuzzy c-means clustering algorithm," Comput. Geosci. **10**(2–3), 191–203 (1984).

[23]M. Medved, M. K. Ivancevic, O. I. Olopade, G. M. Newstead, and G. S. Karczmar, "Echo-planar spectroscopic imaging (EPSI) of the water resonance structure in human breast using sensitivity encoding (SENSE)," Magn. Reson. Med. **63**(6), 1557–1563 (2010).